Reaction Sequences in the Formation of Silico-Ferrites of Calcium and Aluminum in Iron Ore Sinter

NICOLA V.Y. SCARLETT, MARK I. POWNCEBY, IAN C. MADSEN, and AXEL N. CHRISTENSEN

Complex silico-ferrites of calcium and aluminium (low-Fe form, denoted as SFCA; and high-Fe, low-Si form, denoted as SFCA-I) constitute up to 50 vol pct of the mineral composition of fluxed iron ore sinter. The reaction sequences involved in the formation of these two phases have been determined using an *in-situ* X-ray diffraction (XRD) technique. Experiments were carried out under partial vacuum over the temperature range of $T = 22$ °C to 1215 °C (alumina-free compositions) and $T = 22$ °C to 1260 °C (compositions containing 1 and 5 wt pct Al_2O_3) using synthetic mixtures of hematite (Fe_2O_3), calcite ($CaCO_3$), quartz (SiO_2), and gibbsite ($Al(OH)_3$). The formation of SFCA and SFCA-I is dominated by solid-state reactions, mainly in the system CaO-Fe_2O_3. Initially, hematite reacts with lime (CaO) at low temperatures ($T \sim 750$ °C to 780 °C) to form the calcium ferrite phase $2CaO{\cdot}Fe_2O_3$ (C_2F). The C_2F phase then reacts with hematite to produce $CaO{\cdot}Fe_2O_3$ (CF). The breakdown temperature of C_2F to produce the higher-Fe_2O_3 CF ferrite increases proportionately with the amount of alumina in the bulk sample. Quartz does not react with CaO and hematite, remaining essentially inert until SFCA and SFCA-I began to form at around $T = 1050$ °C. In contrast to previous studies of SFCA formation, the current results show that both SFCA types form initially *via* a low-temperature solid-state reaction mechanism. The presence of alumina increases the stability range of both SFCA phase types, lowering the temperature at which they begin to form. Crystallization proceeds more rapidly after the calcium ferrites have melted at temperatures close to $T = 1200$ °C and is also faster in the higher-alumina-containing systems.

I. INTRODUCTION

IRON ore fines are not suitable for direct use in a blast furnace and, so, must first be agglomerated into sinter. In the industrial sintering process, the fine ores (generally, the −1 mm fraction) are mixed with limestone flux and coke breeze and heated to temperatures of around 1220 °C to 1300 °C.[1] Sintering reactions convert the loose raw materials into a porous, but physically strong, cake, which is generally composed of four main phases: iron oxides (~40 to 70 vol pct), ferrites (~20 to 50 vol pct, most of which are a complex silico-ferrite of calcium and aluminium (SCFA)), glasses (up to ~10 vol pct), and dicalcium silicate (up to ~10 vol pct). These agglomerates, or "sinters," have the potential to be quite variable in their composition. However, low-temperature sintering ($T < 1300$ °C) of many hematite-goethite ores, fluxed to a fixed basicity, produces sinters that are reasonably consistent in their mineralogy.

The SFCA is the major bonding phase in iron ore sinter and has been extensively studied on account of its important role in influencing key sinter-quality parameters such as mechanical strength, reducibility,[2,3] and reduction degradation.[4,5] The SFCA can be divided on the basis of composition and morphology into two main types:* one is a low-Fe form that is simply referred to as SFCA, and the second is a high-Fe, low-Si form called SFCA-I.[6] The SFCA-I is a higher-order homologue of SFCA that has a characteristic "platy" morphology, although it may sometimes appear needlelike or acicular in cross section.[6] In contrast, SFCA tends to exhibit a prismatic form, and its morphology has often been referred to as columnar, blocky, or lath shaped.[1,7,8] Typical SFCA-I and SFCA textures are shown in Figure 1. Studies have demonstrated that the type and morphology of the SFCA phase generated depends critically on the chemical composition of the sinter mixture[8,9–11] as well as the processing conditions of sintering.[12,13]

Despite its prevalence and importance, the mechanism of SFCA formation is not fully understood. Previous workers have studied the formation of SFCA using either dynamic scanning electron microscopy (SEM)[14,15] or heat/quench techniques.[16,17] These studies have provided useful information as to the chemical compositions and thermal conditions involved in the creation of SFCA. However, because of the experimental techniques employed, it is difficult to establish the precursor phases or, indeed, which of the homologues of SFCA are formed during the experiments. For example, dynamic SEM experiments provide chemical and textural information regarding the mineralogy, but impart no knowledge as to the crystal structure(s) of the various phases. In comparison, for the heat/quench approach, any short-lived or unquenchable phases, which may be critical to SFCA formation, are not likely to be identified.

In the current study, an *in-situ* X-ray diffraction (XRD) method was used to determine the sequence of reactions involved in the formation of SFCA and SFCA-I. Experiments were conducted on synthetic sinter mixtures within the temperature range of $T = 22$ °C to 1260 °C and using a maximum heating rate of 10 °C/min. This heating rate is considerably slower than those operating during industrial

*Recently, Mumme[18] has described a third SFCA homologue, denoted SFCA-II, synthesized in the ternary CaO-Fe_2O_3-Al_2O_3 system. It is not known if SFCA-II is formed in industrial sinter.

NICOLA V.Y. SCARLETT, MARK I. POWNCEBY, and IAN C. MADSEN are with CSIRO Minerals, Clayton, VIC 3169, Australia. Contact e-mail: nicola.scarlett@csiro.au AXEL N. CHRISTENSEN, Crystal Chemistry, Højkolvej 7, DK-8210 Århus V, Denmark.

Manuscript submitted December 9, 2003.

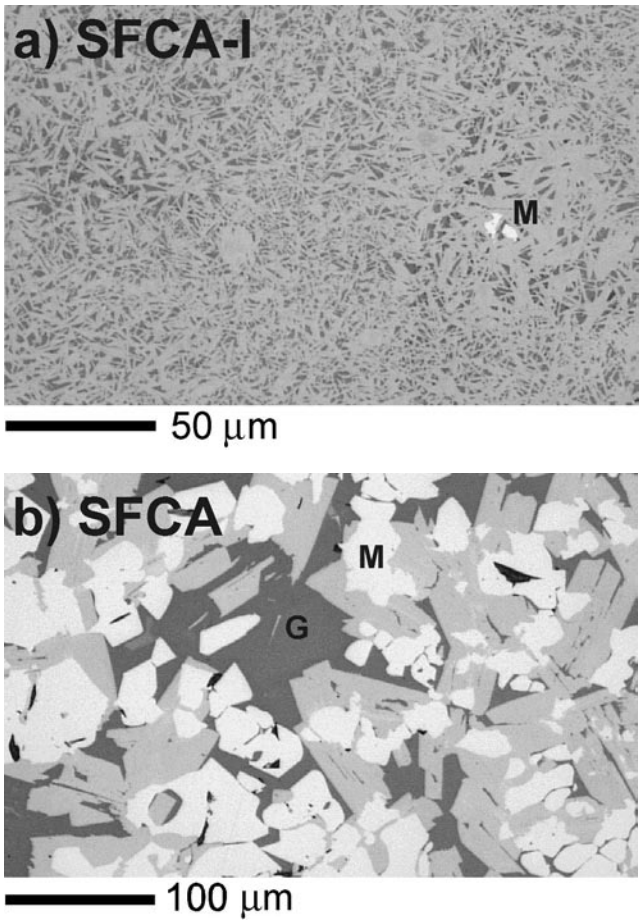

Fig. 1—(*a*) and (*b*) Optical photomicrographs showing typical SFCA-I and SFCA matrix textures in iron ore sinter. In both images, the bright phase is magnetite (M), SFCA-I and SFCA are light gray whilst the dark phase is glass (G). Note the fibrous, meshlike texture of SFCA-I (a) compared to the blocky, columnar texture of SFCA (b).

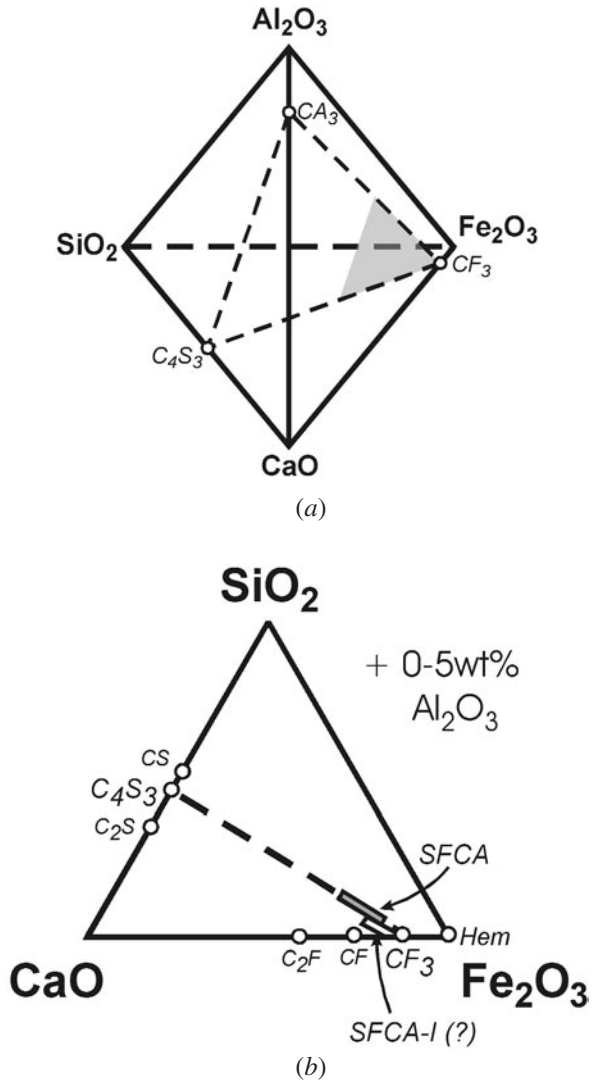

Fig. 2—Schematic diagrams showing (*a*) the compositional plane for SFCA within the Fe_2O_3-Al_2O_3-CaO-SiO_2 quaternary and (*b*) the compositional relationship between SFCA and SFCA-I. In (a), the shaded area shows the region where most SFCA compositions are formed industrial iron ore sinters.

sintering processes, where heating rates of more than 1000 °C/min are typical.[12] The comparatively slow rate used in the current study was necessary to ensure accurate identification and quantification of all phases formed/consumed.

II. EXPERIMENTAL

Starting compositions were designed to lie within a plane that connects the end members CF_3 ($CaO{\cdot}3Fe_2O_3$), CA_3 ($CaO{\cdot}3Al_2O_3$), and C_4S_3 ($4CaO{\cdot}3SiO_2$). According to recent work,[19,20] SFCA forms a limited solid-solution series within this plane. While the compositional plane for SFCA-I is not known, the results of Mumme *et al.*[6] indicate the possibility of intergrowth structures forming between the two end-members of the SFCA group. Diagrams showing the regions of stability for SFCA and SFCA-I (predicted) within the Fe_2O_3-Al_2O_3-CaO-SiO_2 quaternary system are shown in Figure 2.

All experiments were conducted using fine-grained (<2 μm) synthetic mixtures of calcite ($CaCO_3$), hematite (Fe_2O_3), and quartz (SiO_2) that had been doped with varying amounts of alumina (Al_2O_3, added as gibbsite $Al(OH)_3$). The compositional homogeneity of each of the oxide starting materials was confirmed by XRD before mixing. Starting materials were mixed under acetone in a mechanized mortar and pestle for around 40 minutes each (with an intermediate drying and remixing stage) to ensure thorough homogenization. Using these components, three bulk starting mixtures were prepared, in which 0, 1, and 5 wt pct Al_2O_3 had been substituted for Fe_2O_3. These are referred to as samples AL0, AL1, and AL5, respectively. The starting mixtures were limited to compositions containing a maximum of 5 wt pct Al_2O_3, since 5 pct represents the upper level of alumina concentrations measured in SFCAs from industrially produced plant sinter.[11] The compositions of the starting mixtures used are listed in Table I.

Experimental data were obtained using an *in-situ* powder XRD system. An Anton Paar HTK 10 high-temperature chamber was used, employing a platinum resistance-strip heater capable of heating the samples to 1600 °C. The Pt strip contained a small sample well measuring 20.0 × 7.0 × 0.4 mm, and the temperature was measured by a Pt/Pt 10 pct Rh thermocouple connected to the underside of the heating strip. The tem-

perature was calibrated against the solid-solid phase-transition temperature of KNO_3 (128 °C) and the melting points of KNO_3 (333.6 °C), NaCl (804 °C), and NaF (988 °C). Temperatures are considered accurate to ±15 °C. Each sample was sedimented directly onto the Pt strip heater and heated under partial vacuum at a rate of 10 °C per minute to 600 °C (approaching the decomposition temperature of calcite), then at 5 °C per minute to approximately 1260 °C (only to 1215 °C for the AL0 experiment).

The X-ray data were obtained using an X-ray diffractometer incorporating an INEL* CPS-120 curved, position-sensitive

*INEL Z.A., CD 40545410, Artenay, France.

detector. The angular range of the detector is 120 deg 2θ, facilitating rapid, simultaneous data accumulation. Data were collected in the reflection mode using Co K_α radiation. Datasets of 2 minutes in duration were collected continuously throughout each experiment, with up to 100 individual patterns obtained for each sample.

Thermal-analysis measurements were carried out using a SETARAM* Model 92 thermal analyzer, in which approximately

*SETARAM 69300, Caluire, France.

20 mg of starting mixture was loaded into a platinum crucible (8.0-mm o.d., 5.0-mm high) and analyzed against an identical platinum crucible containing an Al_2O_3 reference standard. Both the standard and sample were heated under a flowing atmosphere of high-purity air from ambient temperature to 600 °C at a constant rate of 10 °C per minute and then from 600 °C to 1260 °C at a slower rate of 5 °C per minute (only to 1230 °C for sample AL0). These heating rates are identical to those employed during the *in-situ* XRD measurements. The temperature was monitored using a type-R thermocouple calibrated against the melting point of gold (1064 °C).

Table I. Compositions of Starting Materials

	Oxide (Wt Pct)			
Sample	Fe_2O_3	CaO	SiO_2	Al_2O_3*
AL0	82.36	14.08	3.56	0.00
AL1	81.36	14.08	3.56	1.00
AL5	77.36	14.08	3.56	5.00

*Added as $Al(OH)_3$.

At the completion of the XRD and thermal-analysis experiments, the composition of the resultant SFCA phase(s) was measured using electron-probe microanalysis (EPMA)* methods.

*JEOL JXA-8900R Super probe. JEOL is a trademark of Japan Electron Optics Ltd., Tokyo.

Hematite (Fe_2O_3), wollastonite ($CaSiO_4$), and spinel ($MgAl_2O_4$) were used as standards. Analyses were conducted in wavelength-dispersive mode using an accelerating voltage of 15 kV with a sample current of 25 nA and a beam diameter of 1 to 3 μm. Counting times were of the order of 15 seconds for each element for both the standards and the unknowns. Backscattered-electron images were used to discriminate phases in multiphase assemblages and to locate grain boundaries. Anywhere from 15 to 50 analyses were made on each sample. These data were averaged to give mean phase compositions (Table II).

III. RESULTS AND DISCUSSION

A. *Data Representation*

Results were examined first by stacking all individual 2-minute datasets obtained for each of the three samples. The resulting set of accumulated XRD patterms is illustrated in Figure 3 for the dataset obtained from sample AL5. In this figure, the data are presented as a three-dimensional plot with the diffraction angle (°2θ) along the *x*-axis, temperature (° Celsius) along the *y*-axis, and intensity (counts) represented by a gray scale on the *z*-axis. The view is down the *z*-axis. The discontinuities evident in many of the line traces represent the decomposition of starting materials (*e.g.,* calcite and gibbsite) and short-lived phases (*e.g.,* $Ca_2Fe_2O_5$-C_2F) as the temperature is increased. In subsequent data-refinement procedures, patterns were treated individually as well as in these "stacks," in order to identify all possible phases formed.

B. *Data Refinement*

Full-profile Rietveld refinement using the software package TOPAS*[20] was applied to each of the data sets in order

*TOPAS is a trademark of Bruker AXS, Karlsruhe, Germany.

to quantify the abundance of the various phases. The Rietveld methodology relies upon a wholly crystalline system, in which the structure of all components is known. Note, however,

Table II. Point Analyses of Phases Measured by EPMA on the Residues from DTA and *In-Situ* XRD Experiments; Numbers in Parentheses Represent 2σ Standard Deviation

	Oxide (Wt Pct)					
Sample	Al_2O_3	Fe_2O_3	SiO_2	CaO	Total	Number Analyses
AL0, DTA 1230 °C						
AL0a	—	80.87(0.59)	3.76(0.29)	14.69(0.27)	99.32	16
AL0b	—	81.58(0.66)	3.49(0.47)	14.23(0.49)	99.49	19
AL1, DTA 1260 °C						
AL1	1.42(0.48)	79.06(1.10)	4.02(0.57)	15.40(0.73)	99.89	33
AL5, DTA 1260 °C						
AL5	6.14(0.99)	75.84(1.45)	3.45(0.72)	14.51(0.50)	99.94	35
AL5, in-situ XRD 1260 °C						
AL5	5.78(1.62)	76.81(2.29)	3.71(1.14)	13.69(0.69)	99.99	49

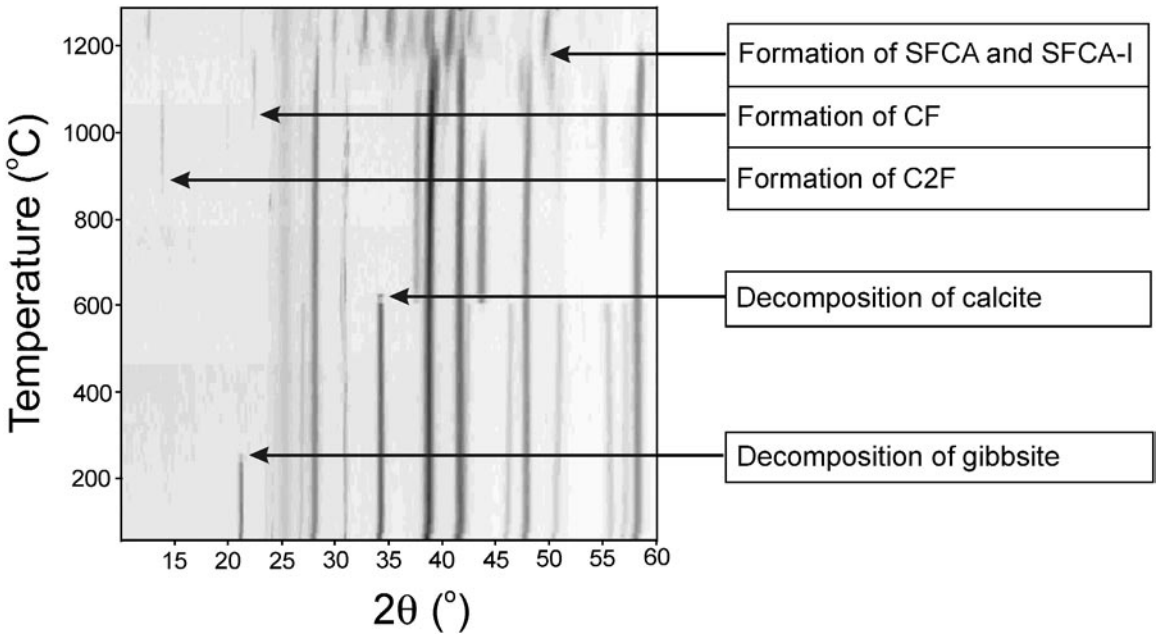

Fig. 3—XRD patterns for experiments with AL5 showing decomposition and subsequent formation of key phases.

that due to the presence of amorphous, poorly structurally defined, or unidentified material produced during reaction (*e.g.,* alumina or a melt phase), it was not possible to report the values of quantification directly from the Rietveld refinements. In the current set of experiments, therefore, quantitative results for each phase were obtained by multiplying the scale factors determined from the Rietveld refinements with a constant derived using the known weight percentages of individual components in the starting mixtures. This absolute method of phase quantification results in totals for each analysis that are generally below 100 pct. The difference between the total and 100 pct is the amount of "unaccounted for" material. This may be composed of amorphous or melt phases, or any unidentified crystalline phases. The amount of material unaccounted for is also further increased by a net loss of material from the sample stage throughout the experiments due to the effects of temperature upon the sample stage (*i.e.,* physical loss of material through thermal spalling).

Figure 4 shows the results of quantitative phase analysis for the three samples examined. All data are consistent in terms of the sequence of phases that form during heating; however, the thermal-stability ranges and abundances of phases formed appear to vary considerably according to the composition of the starting mixture. These are discussed individually as follows.

C. *Phase Formation/Decomposition in the System Fe_2O_3-Al_2O_3-CaO-SiO_2*

1. *Decomposition of gibbsite and calcite*

In experiments where gibbsite was present in the initial mixture (AL1 and AL5), the gibbsite decomposed at a temperature between $T = 240$ °C and 260 °C. Upon decomposition of the gibbsite, peaks corresponding to crystalline alumina were not evident in any of the XRD patterns. This indicates that the alumina is probably present as an amorphous Al oxide. There was no further change in observable phases until the decomposition of calcite to lime (CaO) around $T = 570$ °C to 670 °C.

2. *Formation of $Ca_2Fe_2O_5$ (C_2F)*

From approximately $T = 650$ °C to 675 °C in sample AL0 and $T = 750$ °C to 780 °C in samples AL1 and AL5, $Ca_2Fe_2O_5$ (C_2F) began to form. The hematite and lime concentrations progressively decreased as C_2F formed. The C_2F phase reached a maximum of 19 wt pct in the absence of alumina (AL0) at $T = 920$ °C and a maximum of approximately 22 wt pct in AL1 and AL5 at around $T = 1000$ °C. In the AL0 sample, the C_2F had been consumed before the reaction temperature reached 1050 °C, whereas in both AL1 and AL5, it persisted until in excess of 1100 °C. The higher-temperature stability of C_2F in samples AL1 and AL5 is attributed to Al_2O_3 possibly substituting for Fe_2O_3 in the C_2F structure.

Previous experiments along the Fe_2O_3-CaO binary join[21] confirm the low-temperature stability of the C_2F phase; however, the formation of C_2F as the first new phase to form in the synthesis of SFCA is unexpected based on the bulk starting compositions. The original three compositions all have Fe_2O_3:CaO ratios of greater than 5:1 and, based on the work of Phillips and Muan,[22] the first phase to form should be the $CaFe_2O_4$ (CF) phase. The fact that C_2F forms first between $T = 750$ °C and 780 °C indicates that the dominant reaction mechanism favored at low temperatures is the solid-state reaction between individual CaO and hematite particles.

3. *Formation of $CaFe_2O_4$ (CF)*

In each composition studied, $CaFe_2O_4$ (CF) commenced formation at the peak of C_2F occurrence, between $T = 920$ °C and 1000 °C. In the AL0 system, CF reached a maximum of close to 40 wt pct at $T = 1020$ °C, where it maintained an approximately constant plateau until about $T = 1100$ °C, above which it began to break down. The hematite content mirrored this plateau. In comparison, for the AL1 and AL5 samples, the CF phase reached a maximum of 40 wt pct at

$T = 1145$ °C. The amount of CF began to decline on further heating, and there was no evidence of the CF phase plateau observed in the AL0 mixture. The rate of decline of CF appeared slightly faster in AL5 than AL1. In the AL1 experiment, the rate of hematite consumption diminished as the CF peaked in abundance, while for AL5, the decline of hematite continued steadily throughout the formation and decomposition of CF.

In all compositions studied, CF initially coexisted with C_2F, the latter declining as the amount of CF phase progressively increased. The decomposition of C_2F is explained by the subsequent reaction of the first-formed C_2F with the excess hematite still present in the mixture. The amount of CF reached a maximum when all of the C_2F had been consumed.

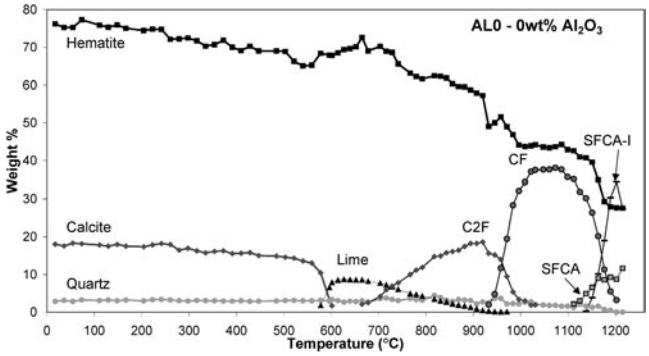

(*a*)

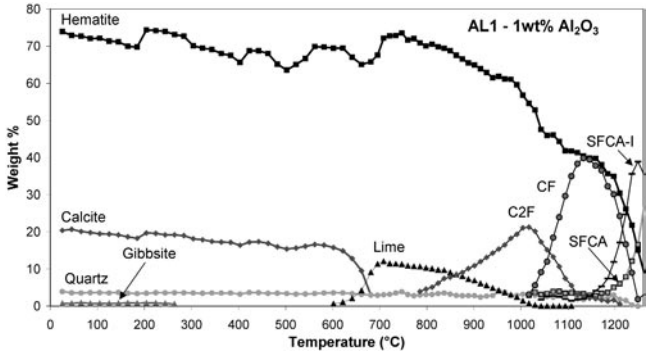

(*b*)

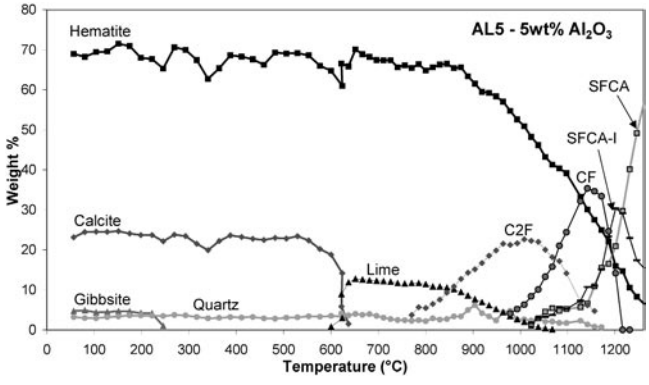

(*c*)

Fig. 4—Results of Rietveld-based quantitative phase analysis of (*a*) AL0-0 wt pct Al_2O_3 substitution, (*b*) AL1-1 wt pct Al_2O_3 substitution, and (*c*) AL5-5 wt pct Al_2O_3 substitution.

In all experiments, the CF phase had completely disappeared by $T = 1200$ °C to 1220 °C. This is in good agreement with the results of Phillips and Muan,[22] who showed that the CF phase is stable only up to $T = 1216$ °C (although they note that a ternary eutectic is present at 1205 °C in mixtures of CF and C_2F).

4. *Formation of SFCA and SFCA-I*

In each experiment, SFCA-1 and SFCA both commenced formation at $T < 1200$ °C. The formation of these SFCA phases coincided with the first evidence of a decrease in the amount of quartz present–quartz is consumed in the SFCA-forming reaction(s).

In the AL0 sample, the formation of SFCA-I and SFCA phase types* both began around $T = 1100$ °C. This initial formation temperature is slightly higher than that predicted by previous results, which showed that SFCA was stable at temperatures above about 1050 °C.[19,23] It should be noted, however, that these studies reflect equilibrium conditions, and run times of up to 28 days (*c.f.* Reference 23) were required in order to produce single-phase SFCA at these temperatures. Clearly, a more rapid heating profile as used in the present study allowed a significant overstepping of the equilibrium SFCA formation temperature before a measurable amount of SFCA was generated.

*In the alumina-free AL0 sample, two SFC phases that are structurally equivalent to SFCA and SFCA-I are present. To preserve continuity with the rest of the text, these phases are both referred to by the SFCA acronym.

Results in Figure 4(a) for the AL0 mixture show that SFCA-I formed at an appreciably faster rate than SFCA. The SFCA-I reached a maximum of approximately 35 wt pct at around $T = 1200$ °C and, thereafter, began to decline. The decrease in SFCA-I abundance corresponds to an increase in the amount of SFCA. The AL0 experiment was not taken beyond $T = 1215$ °C, but, rather, was held at this maximum for 40 minutes to examine the changes in phase abundances with time. Figure 5 shows the quantification of phases in this annealing region of the experiment. The decline of SFCA-I seen in Figure 4(a) continued as a function of time and was associated with an increase in SFCA and consumption of hematite.

In the AL1 and AL5 samples, the formation of both SFCA types commenced at around $T = 1000$ °C. In a similar manner

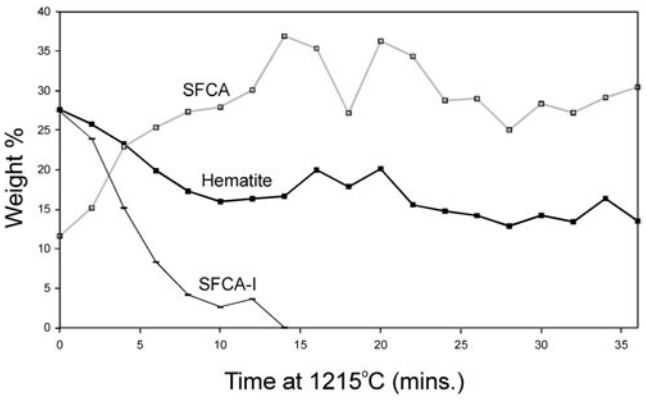

Fig. 5—Results of Rietveld-based quantitative phase analysis of data collected during extended annealing of sample AL0 at T = 1215 °C.

to AL0, SFCA-I reached a maximum first and then was consumed as the rate of formation of SFCA increased. For AL1, the maximum SFCA-I produced is approximately 40 wt pct at $T = 1250$ °C. The corresponding SFCA abundance at this temperature was less than 20 wt pct. In comparison, for AL5, a maximum SFCA-I content of ~30 wt pct was reached at $T = 1200$ °C. The SFCA content at this temperature was also 30 wt pct, implying approximately equal rates of formation. By $T = 1250$ °C, however, AL5 had produced approximately 50 wt pct SFCA (and was increasing) while SFCA-I had decreased to <20 wt pct.

These results indicate that SFCA-I and SFCA formation is more rapid in the higher-alumina-containing AL5 mixture compared to the lower-alumina AL1 and the alumina-free AL0 systems. The alumina also appears to increase the stability range of the SFCA phases by lowering the temperature at which they begin to form.

D. *Thermal Analysis*

The *in-situ* XRD method is not suitable for the detection of any melt phase(s) that may form during heating. To examine if a melt phase is an essential part of SFCA-I and SFCA formation, differential thermal analysis (DTA) measurements were also conducted on all three samples. Results are shown in Figure 6. For all three compositions, the low-temperature ($T <$ 1100 °C to 1150 °C) heat-flow curves are very similar. The main features are (1) a large peak between $T = 730$ °C and 740 °C as carbon dioxide is liberated from calcite, (2) a peak at $T = 240$ °C to 250 °C in mixtures AL1 and AL5, representing the loss of water from gibbsite, and (3) a broad endothermic zone ($T = 760$ °C to 1200 °C) indicating crystallization of calcium ferrites. It is not possible to accurately distinguish formation of C_2F from that of CF, as both phases are present simultaneously (refer to the previous XRD results); however, it is observed that the rate of heat consumption increased slightly between about $T = 1000$ °C to 1100 °C, which may indicate the onset of CF formation.

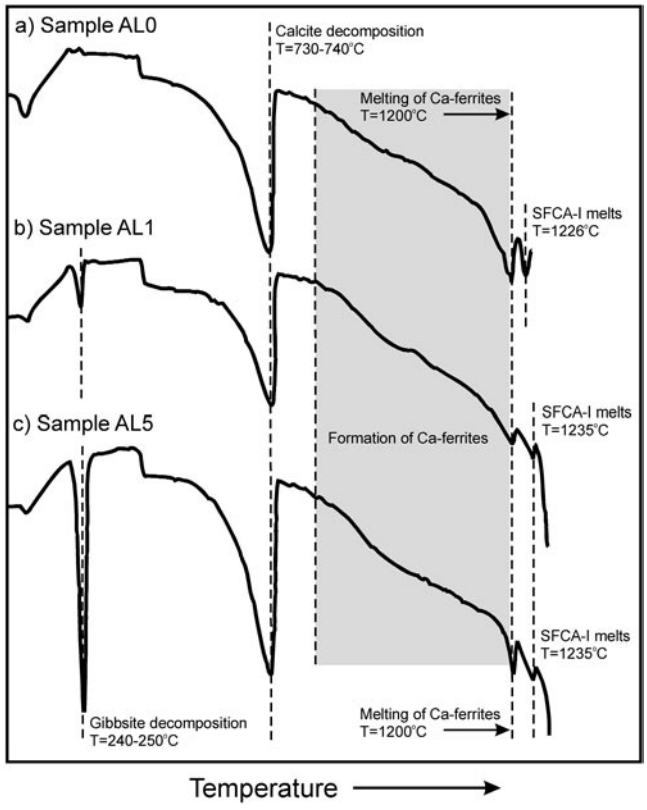

Fig. 6—Differential thermal analysis patterns from samples AL0, AL1, and AL5.

Major differences in the DTA results between the alumina-containing compositions AL1 and AL5 and the alumina-free composition AL0 become apparent at temperatures close to $T = 1200$ °C. These are considered separately as follows.

1. *Composition AL0*

The high-temperature results from the thermal analysis of sample AL0 are more complex to interpret than the two alumina-bearing systems. The heat-flow pattern shows a marked change in slope at $T = 1180$ °C as well as a small double peak close to $T = 1200$ °C. In addition, there is a melting event at $T = 1226$ °C, which most likely represents the decomposition of SFCA-I. The region just below $T = 1200$ °C corresponds to a plateau in both hematite and SFCA abundance (Figure 4(a)), suggesting that some unknown reaction/process may be occurring or that the reaction between hematite and SFCA has ceased. It is noted, however, that DTA measurements by Matsuno[16] on compositions in the Fe_2O_3-CaO-SiO_2 system show similar complexity in this region.

2. *Compositions AL1 and AL5*

Both samples show a strongly endothermic peak at $T = 1198$ °C. This most likely represents the melting of the calcium ferrites, as the peak is close to the eutectic temperature of 1205 °C in the CaO-Fe_2O_3 system.[22] Above 1198 °C, crystallization continues until $T = 1236$ °C, when a second melting event occurs. The second melting event is thought to represent the decomposition of SFCA-I, which is expected to decompose at a lower temperature than SFCA (*e.g.,* Reference 14). This is consistent with the *in-situ* XRD results (Figures 4(b) and (c)). Between 1235 °C and 1260 °C (the maximum temperature of the measurements), SFCA phase continued to crystallize.

E. *The EPMA Examination of Quenched Phases*

The residues from all DTA experiments, as well as a small amount of material from one XRD experiment (the AL5 composition) were recovered and examined using quantitative EPMA.

In all three DTA residues, the major phase present was SFCA (no SFCA-I), with minor amounts of hematite and glass. The presence of SFCA was confirmed by XRD and is consistent with the DTA measurements, which indicated that SFCA-I had decomposed by $T \sim 1226$ °C in AL0 and $T \sim$ 1236 °C in samples AL1 and AL5.

Quantitative EPMA analyses on the residues indicated the bulk of the material to be SFCA of variable composition. Table II and Figure 7 give a summary of the data obtained. Although the data indicate variation in the composition of the SFCA produced, we note that the data cluster closely around the theoretical values based upon the starting materials. The lack of convergence to the theoretical composition reflects lack of equilibrium attained in the experiment, which is to be expected, given the relatively short overall run times.

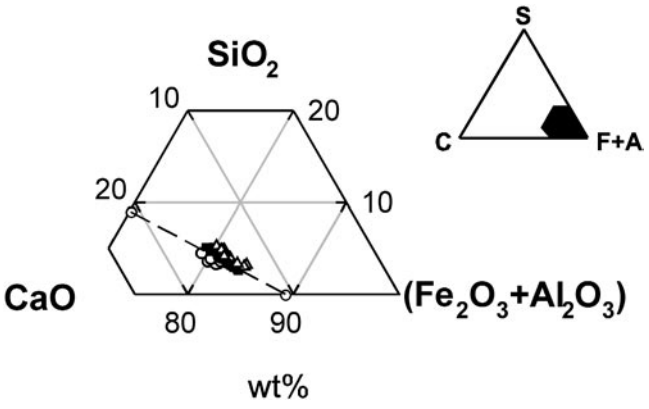

Fig. 7—EPMA data from SFCA samples recovered after XRD and DTA experiments. Symbols used: Δ = 0 wt pct Al_2O_3; ○ = 1 wt pct Al_2O_3; and ■ = 5 wt pct Al_2O_3.

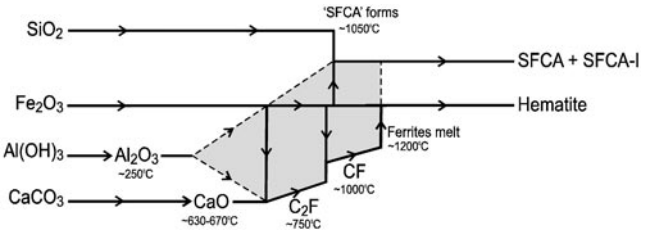

Fig. 8—Schematic diagram showing the reaction sequences involved in the formation of SFCA and SFCA-I.

F. *Comparison with previous work*

Previous workers have studied the formation of SFCA using either dynamic SEM[14] or heat/quench techniques.[16,17] These latter studies examined mixtures of fine powders in the system Fe_2O_3-CaO-SiO_2, which were heated between 900 °C and 1400 °C in air and then rapidly quenched. They showed that up to 1200 °C, reactions occurred in the solid state, with calcium ferrite initially being formed between 950 °C and 1000 °C. At temperatures lower than 1150 °C, SiO_2 hardly reacted with other mineral phases; however, above 1160 °C to 1180 °C, the calcium ferrite melted and reacted with quartz, forming SFCA-I. The study of Hida *et al.*[14] involved a sample of dense iron ore (with or without minor Al_2O_3 and SiO_2) coated with CaO powder and heated in a scanning electron microscope at 300 °C/min under a constant stream of O_2 (10 mL/min). Results showed that Ca-ferrite phases (C_2F and CF) were initially formed *via* solid-state reaction, but as soon as the temperature exceeded 1200 °C, a melt formed and covered the ore surface. Acicular calcium ferrites (SFCA-I) are then quickly formed by the reaction between hematite and the high-CaO melt, absorbing a small amount of SiO_2 and Al_2O_3. Columnar SFCA crystallizes when the temperature rises higher than the melting point of SFCA-I and, further, alumina and silica are assimilated into the melt.

The current work shows that under partial vacuum and at a heating rate of 5 °C/min, SFCA-I and SFCA begin to form at temperatures less than $T = 1200$ °C. Moreover, the formation temperature for both SFCA types is critically dependent on the bulk alumina content, with high-alumina favoring formation temperatures as low as $T = 1000$ °C to 1050 °C. In contrast to previous studies, this implies that SFCA-I and SFCA formation initially begins *via* a solid-state reaction mechanism. The melting of the calcium ferrites at temperatures close to $T = 1200$ °C is still, however, an important stage in the evolution of SFCA bonding phases, as the XRD data indicate that the rate of formation of SFCA-I and SFCA both dramatically increase above 1200 °C. Solid-melt reactions are most likely the dominant reaction mechanism operating at these temperatures, with the presence of a melt phase enhancing the assimilation of the remaining material.

The recognition that SFCA-I and SFCA form at temperatures below $T = 1200$ °C is not consistent with the interpretation of earlier workers, who favored formation temperatures of $T > 1200$ °C.[14,17] It is likely that the conflict with the earlier studies arises through differences in the heating rates used. Although more representative of actual sintering conditions, the high heating rates employed in the earlier studies resulted in phases such as SFCA and SFCA-I, which are both slow to form in the absence of a melt phase, not being recognized until substantial quantities are formed. As indicated earlier, this does not occur until temperatures exceed that of the melting point of the various ferrite phases (*i.e.,* temperatures in excess of $T > 1200$ °C).

C. *Reaction Sequences in the Formation of SFCA*

Based on the results described earlier, the reaction sequences involved in the formation of SFCA phases are summarized schematically in Figure 8. Although an alumina-free composition was studied in the current set of experiments, the reaction sequence in Figure 8 refers to compositions in which alumina is present. This is because most Australian, Indian, and Brazilian ores have $Al_2O_3 > 0.5$ wt pct.[11]

Neglecting the dehydroxylation and decarbonation reactions resulting in the breakdown of gibbsite and calcite, respectively, the formation of SFCA and SFCA-I is dominated by solid-state reactions mainly in the system CaO-Fe_2O_3. Initially, hematite reacts easily with CaO at low temperatures ($T \sim$ 750 °C to 780 °C) to form the calcium ferrite phase C_2F. The C_2F phase then continues to react with hematite, producing CF. The breakdown temperature of C_2F to produce the higher-Fe_2O_3 CF ferrite increases proportionately with the increasing percentage of alumina in the bulk sample. This suggests that the amorphous alumina produced by dehydroxylation of the gibbsite is highly reactive and enters into solid solution with the ferrite phases (indicated by the shaded region in Figure 8). In contrast to alumina, quartz does not react at all with CaO and hematite, remaining essentially inert until SFCA and SFCA-I begin to form around $T =$ 1050 °C. The SFCA formation is dependent upon alumina content, with SFCA and SFCA-I forming at lower temperatures in high-Al_2O_3 systems. The rate of SFCA formation is also enhanced in systems with higher alumina contents. If the temperature of sintering exceeds approximately $T =$ 1220 °C to 1240 °C, SFCA-I breaks down, leaving SFCA and hematite as the product phases.

IV. SUMMARY

The formation of the sinter phases SFCA and SFCA-I has been studied using a combination of *in-situ* XRD, DTA, and

EPMA techniques. The mineral formation processes were established using synthetic mixtures of hematite, calcite, quartz, and gibbsite powders. Results obtained are summarized as follows

1. Phase formation is dominated by solid-state reactions, mainly in the system $CaO\text{-}Fe_2O_3$. Hematite initially reacts with CaO at low temperatures ($T \sim 750$ °C to 780 °C) to form the calcium ferrite phase C_2F. The C_2F phase then continues to react with hematite, producing CF ($T \sim 920$ °C to 1000 °C). The CF is stable up to $T \sim 1200$ °C. The presence of alumina increases the temperature at which both ferrite phases initially form.
2. Quartz does not react at all with CaO and hematite, remaining essentially inert until SFCA and SFCA-I begin to form around $T = 1050$ °C. The formation of both SFCA types proceeds initially *via* a solid-state reaction mechanism.
3. The SFCA-I and SFCA formation is more rapid in the higher-alumina-containing systems. The presence of alumina increases the stability range of both SFCA phase types, lowering the temperature at which they begin to form.

The current results are specific to the compositions, grain size, heating rates, and sintering environment used. Industrial sintering processes, however, operate under more-reduced oxygen atmospheres,[24,25] have a coarser grain size, and have a more rapid heating profile.[1] In addition, the ore is generally contaminated by minor amounts of impurities such as MgO, MnO, or S. Further work is needed to assess the impact of all these factors on the amount and type of SFCA generated.

ACKNOWLEDGMENTS

Appreciation is expressed to fellow CSIRO Minerals staff members including Colin Mac Rae (electron microprobe), Luda Malishev (sample preparation), John Clout (images in Figure 1), and Terry Hall (DTA). Thanks are also extended to John Clout and Graham Sparrow (both at CSIRO Minerals) who provided critical reviews of earlier versions of this article. ANC also acknowledges the Aarhus University Research Foundation Grant No. E-2001-NAT-1-4-LP.

REFERENCES

1. M. Sasaki and Y. Hida: *Tetsu-to-Hagané,* 1982, vol. 68, pp. 563-71 (in Japanese).
2. K. Kitamura, F. Shigemori, Y. Hatakeyama, T. Kawaguchi, and K. Takata: *AIME Ironmaking Proc.,* 1985, vol. 44, pp. 405-14.
3. N.J. Bristow and A.G. Waters: *Trans. Inst. Min. Metall. (Sect. C: Mineral Processing Extr. Metall.),* 1991, vol. 100, pp. C1-C10.
4. I. Shigaki, M. Sawada, and N. Gennai: *Trans. Iron Steel Inst. Jpn.,* 1986, vol. 26, pp. 503-11.
5. C.E. Loo, K.T. Wan, and V.R. Howes: *Ironmaking and Steelmaking,* 1988, vol. 15, pp. 279-85.
6. W.G. Mumme, J.M.F. Clout, and R.W. Gable: *Neues Jahrbuch Miner. Abh,* 1988, vol. 173, pp. 93-117.
7. SN. Ahsan, T. Mukherjee, and J.A. Whiteman: *Ironmaking and Steelmaking,* 1983, vol. 10, pp. 54-64.
8. P.R. Dawson, J. Ostwald, and K.M. Hayes: *Trans. Inst. Min. Metall. (Sect. C: Mineral Processing Extr. Metall.),* 1985, vol. 94, pp. C71-C78.
9. P.R. Dawson, J. Ostwald, and K.M. Hayes: *BHP Tech. Bull.,* 1983, vol. 27, pp. 47-51.
10. T. Mukherjee and J.A. Whiteman: *Ironmaking and Steelmaking* 1985, vol. 12, pp. 151-56.
11. M.I. Pownceby and J.M.F. Clout: *Trans. Inst. Min. Metall. (Sect. C: Mineral Processing Extr. Metall.),* 2003, vol. 112, pp. C44-C51.
12. P.R. Dawson, J. Ostwald, and K.M. Hayes: *Proc. Aus. Inst. Min. Metall.,* 1984, vol. 289, pp. 163-69.
13. Y. Hida, J. Okazaki, K. Itoh, and M. Sasaki: *Tetsu-to-Hagané,* 1987a, vol. 73, pp. 91-98 (in Japanese).
14. Y. Hida, M. Sasaki, K. Sato, M. Kagawa, M. Takeshi, H. Soma, H. Naito, and M. Taniguchi: *Nippon Steel Tech. Rep.,* 1987b, vol. 35, pp. 59-67.
15. Y. Hida, T. Inazumi, K. Sato, and M. Sugata: *Proc. 5th China–Japan Symp. on Science and Technology of Iron and Steel,* International Academic Publishers, Beijing, 1989, pp. 96-107.
16. F. Matsuno: *Trans. Iron Steel Inst. Jpn.,* 1979, vol. 19, pp. 595-604.
17. F. Matsuno and T. Harada: *Trans. Iron Steel Inst. Jpn.,* 1981, vol. 21, pp. 318-325.
18. W.G. Mumme: *Neues Jahrbuch Miner. Abh.,* 2003, vol. 178, pp. 307-335.
19. J.D.G. Hamilton, B.F. Hoskins, W.G. Mumme, W.E. Borbidge, and M.A. Montague: *Neues Jahrbuch Miner. Abh.,* 1989, vol. 161, pp. 1-26.
20. Bruker AXS: *TOPAS V2.1: General Profile and Structure Analysis Software for Powder Diffraction Data,* Bruker AXS, Karlsruhe, Germany, 2003.
21. T.R.C. Patrick and M.I. Pownceby: *Metall. Mater. Trans. B,* 2002, vol. 33B, pp. 79-89.
22. B. Phillips and A. Muan: *J. Am. Ceram. Soc.,* 1959, vol. 42, pp. 413-23.
23. M.I. Pownceby and T.R.C. Patrick: *Eur. J. Mineralogy,* 2000, vol. 12, pp. 455-68.
24. L.-H. Hsieh and J.A. Whiteman: *Trans. Iron Steel Inst. Jpn.,* 1989a, vol. 29, pp. 24-32.
25. L.-H. Hsieh and J.A. Whiteman: *Trans. Iron Steel Inst. Jpn.,* 1989b, vol. 29, pp. 625-34.